ARL-CR-0839 ● SEP 2019

Distributed Kalman Filters for Cooperative Localization of Munition Swarms

by Bradley T Burchett
Rose-Hulman Institute of Technology
Terre Haute, Indiana

under contract W911NF-19-2-0199

NOTICES

Disclaimers

The findings in this report are not to be construed as an official Department of the Army position unless so designated by other authorized documents.

Citation of manufacturer's or trade names does not constitute an official endorsement or approval of the use thereof.

Destroy this report when it is no longer needed. Do not return it to the originator.

ARL-CR-0839 ● SEP 2019

Distributed Kalman Filters for Cooperative Localization of Munition Swarms

Bradley T Burchett
Rose-Hulman Institute of Technology
Terre Haute, Indiana

under contract W911NF-19-2-0199

REPORT DOCUMENTATION PAGE

Form Approved
OMB No. 0704-0188

1. REPORT DATE *(DD-MM-YYYY)*	2. REPORT TYPE	3. DATES COVERED (From - To)
September 2019	Contractor Report	June–August 2019

4. TITLE AND SUBTITLE
Distributed Kalman Filters for Cooperative Localization of Munition Swarms

5a. CONTRACT NUMBER
W911NF-19-2-0199

5b. GRANT NUMBER

5c. PROGRAM ELEMENT NUMBER

6. AUTHOR(S)
Bradley T Burchett

5d. PROJECT NUMBER

5e. TASK NUMBER

5f. WORK UNIT NUMBER

7. PERFORMING ORGANIZATION NAME(S) AND ADDRESS(ES)
Rose-Hulman Institute of Technology
5500 Wabash Ave
Terre Haute, IN 47803

8. PERFORMING ORGANIZATION REPORT NUMBER
ARL-CR-0839

9. SPONSORING/MONITORING AGENCY NAME(S) AND ADDRESS(ES)
CCDC Army Research Laboratory
ATTN: FCDD-RLW-LE
Aberdeen Proving Ground, MD 21005

10. SPONSOR/MONITOR'S ACRONYM(S)

11. SPONSOR/MONITOR'S REPORT NUMBER(S)

12. DISTRIBUTION/AVAILABILITY STATEMENT
Approved for public release; distribution is unlimited.

13. SUPPLEMENTARY NOTES
ORCID ID: Bradley T Burchett, 0000-0002-1934-0537

14. ABSTRACT

Cooperative localization is a way for munition swarms to navigate in areas where GPS is denied or degraded. Cooperative schemes seek to distribute sensing and computing tasks among members of the swarm so that several agents with simpler, cheaper sensors and processors achieve high-precision solutions. Range-only sensors tend to be simpler, cheaper, and more rugged, thus this work considers only slant-range measurements between agents. Formulations of the distributed extended and unscented Kalman filters are reviewed in the context of range-only cooperative navigation. Measurement update equations are updated specific to the distributed extended Kalman filter for range-only measurements. Computational and communication sequences are clarified for distributed algorithms in formations larger than three. Several case studies are simulated to test for system observability and demonstrate performance of the algorithms.

15. SUBJECT TERMS
cooperative localization, nonlinear Kalman Filter, distributed sensing, distributed filtering, munition swarms

16. SECURITY CLASSIFICATION OF:			17. LIMITATION OF ABSTRACT	18. NUMBER OF PAGES	19a. NAME OF RESPONSIBLE PERSON
a. REPORT	b. ABSTRACT	c. THIS PAGE			Bradley T Burchett
Unclassified	Unclassified	Unclassified	UU	37	19b. TELEPHONE NUMBER (Include area code) (410) 278-2479

Contents

List of Figures

List of Tables

1. Introduction

Cooperative localization is a way for munition swarms to navigate in areas where GPS is denied or degraded. Cooperative schemes seek to distribute sensing and computing tasks among members of the swarm so that several agents with simpler, cheaper sensors and processors achieve high-precision solutions. Range-only sensors tend to be simpler, cheaper and more rugged, thus this work considers only slant-range measurements between agents. Cooperative localization has been investigated extensively in the robotics community for land-based robots navigating in a planar space. Recently, applications to unmanned aerial vehicles (UAVs) and spacecraft navigating in 3-D space have been presented.[1–4]

Efforts to decentralize the Kalman filter were initiated with the work of Roumeliotis and Bekey.[5] They decentralized the discrete time Kalman filter for linearized state propagation and measurement equations. Their work used relative pose measurements among a group of three robots navigating in a plane.

About the same time, Julier and Uhlmann introduced the unscented Kalman filter (UKF) through various contributions across the broad controls community.[6] Building on these two disruptive ideas, various researchers have since developed sigma-point information filters (sIFs),[7] distributed UKF,[8] and distributed sIF.[7]

In this work, we seek to leverage the distributed UKF with nonlinear state dynamics and measurement models to ensure system observability with minimum dimension state and measurement vectors. The distributed extended Kalman filter (EKF) is reviewed and expanded, clarifying the sequence of calculations for formations larger than three agents using range-only measurements. Previous studies[9,10] have shown the linearization of state and measurement dynamics in the EKF can prevent it from achieving theoretically predicted nonlinear observability. Thus, the distributed UKF is then presented in the context of range-only exteroceptive measurements and limited proprioceptive measurements, and expanded for teams larger than three agents.

This report proceeds as follows. Section 2 reviews and expands the distributed Kalman filter method to nonlinear models and formations of more than three agents. Section 3 proposes a scalable UKF for large formations. Section 4 presents results of the algorithms.

2. Review and Expansion of Distributed EKF

2.1 Centralized EKF

Given a set of nonlinear plant dynamics

$$\dot{\mathbf{x}} = \mathbf{f}(\mathbf{x}, \mathbf{u}) + \mathbf{v} \tag{1}$$

and measurement model

$$\mathbf{y} = \mathbf{h}(\mathbf{x}) + \mathbf{w}\,. \tag{2}$$

The EKF provides a recursive estimation scheme for systems described by nonlinear dynamics such as Eqs. 1 and 2. It consists of a prediction (a priori) step prior to measurement, and correction (a posteriori) step after measurement. The state estimate mean and covariance are propagated through the system dynamics in the prediction step

$$\hat{\mathbf{x}}_{k+1} = \mathbf{\Phi}\hat{\mathbf{x}}_k + \mathbf{\Gamma}\mathbf{u}_k \tag{3}$$

$$\mathbf{P}_{k+1}^{-} = \mathbf{\Phi}\mathbf{P}_{\mathbf{k}}^{+}\mathbf{\Phi}^T + \mathbf{Q}\,, \tag{4}$$

where $\mathbf{\Phi}$ is the state transition matrix $\mathbf{\Phi} = \exp(\mathbf{A}T)$. $\mathbf{A}$ is the state dynamics Jacobian $\mathbf{A} = \partial\mathbf{f}/\partial\mathbf{x}$. $\mathbf{Q}$ is the process noise covariance matrix $\mathbf{Q} = \mathbf{E}[\mathbf{v}\mathbf{v}^T]$.

After measurement, the a posteriori estimate and covariance are found through the following sequence of calculations

$$\mathbf{S} = \mathbf{H}\mathbf{P}_{k+1}^{-}\mathbf{H}^T + \mathbf{R} \tag{5}$$

$$\mathbf{K} = \mathbf{P}_{k+1}^{-}\mathbf{H}^T\mathbf{S}^{-1} \tag{6}$$

$$\hat{\mathbf{x}}_{k+1}^{+} = \hat{\mathbf{x}}_{k+1}^{-} + \mathbf{K}(\mathbf{y}_{k+1} - \hat{\mathbf{y}}_{k+1}) \tag{7}$$

$$\mathbf{P}_{k+1}^{+} = \mathbf{P}_{k+1}^{-} - \mathbf{K}\mathbf{S}\mathbf{K}^T\,, \tag{8}$$

where $\hat{\mathbf{y}}_{k+1} = \mathbf{h}(\hat{\mathbf{x}}_{k+1})$, $\mathbf{H}$ is the measurement Jacobian $\mathbf{H} = \partial\mathbf{h}/\partial\mathbf{x}$, and $\mathbf{R}$ is the measurement noise covariance $\mathbf{R} = \mathbf{E}[\mathbf{w}\mathbf{w}^T]$.

2.2 Distributed EKF

Roumeliotis and Bekey[5] reformulated the Kalman filter equations to allow distributed evaluation among a group of cooperating agents. If the individual agent's dynamics can be written as

$$\dot{\boldsymbol{x}}_p = \begin{Bmatrix} \dot{x}_p \\ \dot{y}_p \\ \dot{\psi}_p \end{Bmatrix} = \begin{Bmatrix} V_p \cos\psi_p \\ V_p \sin\psi_p \\ \omega_p \end{Bmatrix} \tag{9}$$

in planar motion, or

$$\dot{\boldsymbol{x}}_p = \begin{Bmatrix} \dot{x}_p \\ \dot{y}_p \\ \dot{z}_p \\ \dot{\psi}_p \\ \dot{\theta}_p \\ \dot{V}_p \end{Bmatrix} = \begin{Bmatrix} V_p \cos\psi_p \cos\theta_p \\ V_p \sin\psi_p \cos\theta_p \\ -V_p \sin\theta_p \\ r_p \\ q_p \\ -g \sin\gamma_p \end{Bmatrix}$$

in 3-D, all team pose states are concatenated in a common system state vector $\mathbf{x} = [x_p, y_p, \psi_p \quad x_q, y_q, \psi_q, \quad \cdots]^T$. Terms in Eqs. 5–8 can then be conformably partitioned between agents making up the formation.

$$\mathbf{P} = \begin{bmatrix} \mathbf{P}_{pp} & \mathbf{P}_{pq} & \cdots \\ \mathbf{P}_{qp} & \mathbf{P}_{qq} & \cdots \\ \vdots & \vdots & \ddots \end{bmatrix}$$

$$\mathbf{H} = [\mathbf{H}_p \quad \mathbf{H}_q \quad \cdots]$$

$$\mathbf{K} = \begin{bmatrix} \mathbf{K}_p \\ \mathbf{K}_q \\ \vdots \end{bmatrix}$$

$$\hat{\mathbf{x}}_{k+1}^{+} = \begin{Bmatrix} \hat{\mathbf{x}}_{k+1}^{p+} \\ \hat{\mathbf{x}}_{k+1}^{q+} \\ \vdots \end{Bmatrix}$$

If an agent measures its neighbor's relative pose in a common frame, then the measurement can be written as a linear combination of system states; that is,

$$\mathbf{y} = \begin{Bmatrix} x_p - x_q \\ y_p - y_q \\ \psi_p - \psi_q \end{Bmatrix} = [0 \quad \cdots \quad \mathbf{I} \quad \cdots \quad 0 \quad \cdots \quad -\mathbf{I} \quad \cdots \quad 0]\{\mathbf{x}\} \tag{10}$$

or

$$\mathbf{H} = [0 \quad \cdots \quad \mathbf{I} \quad \cdots \quad 0 \quad \cdots \quad -\mathbf{I} \quad \cdots \quad 0].$$

For range-only measurements,

$$\mathbf{y}_k = \mathbf{h}_k(\mathbf{x}_p, \mathbf{x}_q) = \sqrt{(x_p - x_q)^2 + (y_p - y_q)^2 + (z_p - z_q)^2}$$

and

$$\mathbf{H}_{pq} = \begin{bmatrix} 0 & \cdots & \dfrac{\partial \mathbf{h}}{\partial \mathbf{x}_p} & \cdots & 0 & \cdots & \dfrac{\partial \mathbf{h}}{\partial \mathbf{x}_q} & \cdots & 0 \end{bmatrix} \tag{11}$$

since measurements are defined between agents q and p.

Roumeliotis and Bekey's primary contribution was to decompose Eq. 4 for off-diagonal blocks of the system state covariance matrix.[5] For on-diagonal blocks, $\mathbf{P}^-_{pp,k+1} = \mathbf{\Phi}_p \mathbf{P}^+_{pp,k} \mathbf{\Phi}_p^T + \mathbf{Q}_p$, the propagation depends only upon the dynamics of agent p. Off-diagonal elements will depend upon robots p and q for $\mathbf{P}_{pq}$. By decomposing the term

$$\mathbf{\Phi}_p \mathbf{P}^+_{pq,k} \mathbf{\Phi}_q^T = \mathbf{\Phi}_p \sqrt{\mathbf{P}^+_{pq,k}} \sqrt{\mathbf{P}^{T+}_{qp,k}} \mathbf{\Phi}_q^T, \tag{12}$$

it is then possible to propagate the matrix square root of the off-diagonal covariance terms. The singular value decomposition can be used to find two matrix square roots corresponding to the row and column spaces of $\mathbf{P}_{pq}$. That is

$$\mathbf{P}^+_{pq,k} = \mathbf{U}_{pq} \mathbf{W}_{pq} \mathbf{V}^T_{pq} = (\mathbf{U}_{pq} \mathbf{W}_i)(\mathbf{V}_{pq} \mathbf{W}_j)^T , \tag{13}$$

where $\mathbf{W}_i = \mathbf{W}_j = \sqrt{\mathbf{W}_{pq}}$. Then

$$\mathbf{P}^-_{pq,k+1} = \mathbf{\Phi}_p (\mathbf{U}_{pq} \mathbf{W}_p) \cdot (\mathbf{V}_{pq} \mathbf{W}_q)^T \mathbf{\Phi}_q^T = \mathbf{P}_{i,pq} \cdot \mathbf{P}^T_{j,pq} , \tag{14}$$

such that the left factor is propagated through the dynamics of agent p, and the right factor is propagated through the dynamics of agent q. In formations larger than three agents, an extra measure of computational efficiency is realized by propagating the row and column spaces as shown in Eq. 14.

2.3 A Priori Updates for Formations Larger than Three Agents

Given the row/column space decomposition for the a priori propagation of off-diagonal blocks, a formation of three agents will require the propagation of all possible permutations of row and column spaces

$$\{i,j\} = \{p,q\},\{q,r\},\{r,p\}\,.$$

That is,

$$\mathbf{U}_{pq}, \mathbf{W}_p, \mathbf{V}_{rp}, \mathbf{W}_r, \rightarrow \mathbf{P}^-_{pp,k+1}, \mathbf{P}_{i,pq}, \mathbf{P}_{j,rp}, \mathbf{\Phi}_p$$

$$\mathbf{U}_{qr}, \mathbf{W}_q, \mathbf{V}_{pq}, \mathbf{W}_p, \rightarrow \mathbf{P}^-_{qq,k+1}, \mathbf{P}_{i,qr}, \mathbf{P}_{j,pq}, \mathbf{\Phi}_q \tag{15}$$

$$\mathbf{U}_{rp}, \mathbf{W}_r, \mathbf{V}_{qr}, \mathbf{W}_q, \rightarrow \mathbf{P}^-_{rr,k+1}, \mathbf{P}_{i,rp}, \mathbf{P}_{j,qr}, \mathbf{\Phi}_r\,,$$

and the off-diagonal elements are then assembled from the row and column spaces, for instance

$$\mathbf{P}^-_{pq,k+1} = \mathbf{P}_{i,pq} \cdot \mathbf{P}^T_{j,pq}, \text{ and } \mathbf{P}^-_{qp,k+1} = \mathbf{P}^{T-}_{pq,k+1}\,.$$

For larger formations, the entire set of off-diagonal blocks can be computed by propagating the row and column spaces of the first block superdiagonal and the bottom left corner. Thus, the dynamics of each agent are used to propagate one diagonal block, one row space, and one column space. Figure 1 illustrates the computational flow for a five-agent example.

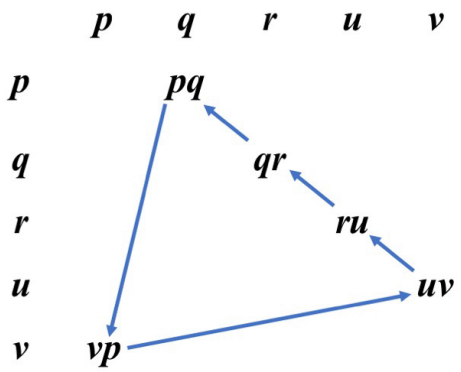

Fig. 1 Off-diagonal blocks of the system covariance matrix required to propagate the entire off-diagonal space. By propagating the row and column spaces of the illustrated terms, all off-diagonal blocks may be reconstructed.

Thus, after decomposing the blocks illustrated in Fig. 1, the following inputs are used to propagate the terms shown on the right-hand side of each expression

$$\begin{gathered}
\mathbf{U}_{pq}, \mathbf{W}_p, \mathbf{V}_{vp}, \mathbf{W}_v, \rightarrow \mathbf{P}_{pp}, \mathbf{P}_{i,pq}, \mathbf{P}_{j,vp}, \boldsymbol{\Phi}_p \\
\mathbf{U}_{qr}, \mathbf{W}_q, \mathbf{V}_{pq}, \mathbf{W}_p, \rightarrow \mathbf{P}_{qq}, \mathbf{P}_{i,qr}, \mathbf{P}_{j,pq}, \boldsymbol{\Phi}_q \\
\mathbf{U}_{ru}, \mathbf{W}_r, \mathbf{V}_{qr}, \mathbf{W}_q, \rightarrow \mathbf{P}_{rr}, \mathbf{P}_{i,ru}, \mathbf{P}_{j,qr}, \boldsymbol{\Phi}_r \\
\mathbf{U}_{uv}, \mathbf{W}_u, \mathbf{V}_{ru}, \mathbf{W}_r, \rightarrow \mathbf{P}_{uu}, \mathbf{P}_{i,uv}, \mathbf{P}_{j,ru}, \boldsymbol{\Phi}_u \\
\mathbf{U}_{vp}, \mathbf{W}_v, \mathbf{V}_{uv}, \mathbf{W}_u, \rightarrow \mathbf{P}_{vv}, \mathbf{P}_{i,vp}, \mathbf{P}_{j,uv}, \boldsymbol{\Phi}_v \quad ,
\end{gathered} \tag{16}$$

and the first superdiagonal terms can be reconstructed from the row and column spaces shown (i.e., $\mathbf{P}^-_{pq,k+1} = \mathbf{P}_{i,pq} \cdot \mathbf{P}^T_{j,pq}$). Terms above the first superdiagonal can then be explicitly computed using both state transition matrices $\boldsymbol{\Phi}_p \mathbf{P}^+_{pr,k} \boldsymbol{\Phi}^T_r$. Once the upper block-triangular part of $\mathbf{P}^-_{k+1}$ is computed, the blocks below the diagonal are filled by reflecting blocks across the diagonal.

2.4 A Posteriori Updates

Since interagent measurements only involve two agents at a time, the measurement sensitivity can be written as in Eq. 11 and only two blocks will be nonzero as shown. Substituting Eq. 11 into Eqs. 5–7 results in

$$\mathbf{S}_{pq} = \frac{\partial \mathbf{h}}{\partial \mathbf{x}_p}\left(\mathbf{P}_{pp}\frac{\partial \mathbf{h}^T}{\partial \mathbf{x}_p} + \mathbf{P}_{pq}\frac{\partial \mathbf{h}^T}{\partial \mathbf{x}_q}\right) + \frac{\partial \mathbf{h}}{\partial \mathbf{x}_q}\left(\mathbf{P}_{qp}\frac{\partial \mathbf{h}^T}{\partial \mathbf{x}_p} + \mathbf{P}_{qq}\frac{\partial \mathbf{h}^T}{\partial \mathbf{x}_q}\right) \tag{17}$$

$$\mathbf{P}^+_{ij} = \mathbf{P}^-_{ij} - \left(\mathbf{P}^-_{ip}\frac{\partial \mathbf{h}^T}{\partial \mathbf{x}_p} + \mathbf{P}^-_{nq}\frac{\partial \mathbf{h}^T}{\partial \mathbf{x}_q}\right)\mathbf{S}^{-1}_{pq}\left(\frac{\partial \mathbf{h}}{\partial \mathbf{x}_p}\mathbf{P}^-_{pm} + \frac{\partial \mathbf{h}}{\partial \mathbf{x}_q}\mathbf{P}^-_{qm}\right) \tag{18}$$

$$\mathbf{K} = \begin{bmatrix} \left(\mathbf{P}_{1p}\frac{\partial \mathbf{h}^T}{\partial \mathbf{x}_p} + \mathbf{P}_{1q}\frac{\partial \mathbf{h}^T}{\partial \mathbf{x}_q}\right)\mathbf{S}^{-1}_{pq} \\ \left(\mathbf{P}_{2p}\frac{\partial \mathbf{h}^T}{\partial \mathbf{x}_p} + \mathbf{P}_{2q}\frac{\partial \mathbf{h}^T}{\partial \mathbf{x}_q}\right)\mathbf{S}^{-1}_{pq} \\ \vdots \end{bmatrix} \tag{19}$$

$$\hat{\mathbf{x}}_{k+1}^{p+} = \hat{\mathbf{x}}_{k+1}^{p-} + \mathbf{K}^{p}(\mathbf{y}_{k+1} - \hat{\mathbf{y}}_{k+1}) \,. \tag{20}$$

These results are demonstrated in the Section 4 through simulations where interagent measurements are intermittent.

3. Distributed UKF

Previous studies have shown that linearization of the system dynamics prevents EKF schemes from achieving theoretical nonlinear observability.[9,10] This situation can be remedied by increasing model fidelity through increasing model state dimension, or increasing the number of measurements. A previous work showed that in 3-D flight, a nine-state per agent model is adequate for observability when using range-only measurements.[10] However, an accompanying work showed that the UKF can achieve observability using only a six-state per agent model.[9]

The UKF is a nonderivative filter which propagates a distribution of solutions through the nonlinear system dynamics and thus preserves theoretical observability.

3.1 Propagating the A Priori State Estimate through Sigma Points

Given $\mathbf{P}_k^+$, **R**, and **Q,** concatenate

$$\mathbf{\Sigma} = \frac{N_x}{1-w_m^{(0)}} \begin{bmatrix} \mathbf{P}_k^+ & & \\ & \mathbf{Q} & \\ & & \mathbf{R} \end{bmatrix}. \tag{21}$$

The sigma points are based upon the square root of matrix **Σ.** In order to distribute calculation of the sigma points among several agents, we capitalize upon two properties of **Σ**. First, the **Q** and **R** matrices are defined to be diagonal, so their corresponding square roots are simply the scalar square roots of their diagonal elements. Second, a Cholesky factorization is used on the $\mathbf{P}_k^+$ as described in Dinh and Kia[8] except that a lower triangular decomposition is preferred. Consider the case $\mathbf{L}\mathbf{L}^T = \mathbf{A}$**,** where **L** is lower triangular. If **A** is partitioned as[11]

$$\mathbf{A} = \begin{bmatrix} \mathbf{P} & \mathbf{q} \\ \mathbf{q}^T & \mathbf{r} \end{bmatrix},$$

then the matrix **P** has the Cholesky factorization $\mathbf{P} = \mathbf{L_P}\mathbf{L_P}^T$ and

$$\mathbf{L} = \begin{bmatrix} \mathbf{L_P} & 0 \\ \mathbf{w}^T & \mathbf{t} \end{bmatrix},$$

where $\mathbf{L_P w} = \mathbf{q}$ and $\mathbf{t} = \sqrt{\mathbf{r} - \mathbf{w}^T\mathbf{w}}$. Thus, although the factorization is not entirely distributable, it can be done a row at a time. Thus $\mathbf{L}\mathbf{L}^T = \mathbf{P}_k^+$ and each agent will operate on blocks of $\mathbf{L}$ rather than $\mathbf{P}_k^+$. Define $\mathbf{L}^p$ as the rows of $\mathbf{L}$ corresponding to the states of agent *p*. Since $\mathbf{L}^p$ is already a square root matrix, the sigma points for agent *p* can be found as

$$\mathbf{X}_{i,k}^p = \begin{cases} \mathbf{x}_k^p, i = 0 \\ \mathbf{x}_k^p + \mathbf{L}_i^p, i = 1, \dots, N \\ \mathbf{x}_k^p - \mathbf{L}_i^p, i = N+1, \dots, 2N \end{cases},$$

where $\mathbf{A}_i$ is the *i*th column of the $\mathbf{A}$ matrix. Transform the sigma points through the state-update function,

$$\mathbf{X}_{i,k+1}^{p-} = f(\mathbf{X}_{i,k}^p, \mathbf{u}_k), \ i = 0,1, \dots, 2N \ .$$

For continuous-time equations, this step can be performed using a Runge–Kutta time marching scheme. Process noise is then added to columns of the state sigma points matrix $\mathbf{X}_{k+1}^{p-} = \mathbf{X}_{k+1}^{p-} \pm \sqrt{\mathbf{Q}}$.

Calculate the a priori state estimate and a priori covariance:

$$\hat{\mathbf{x}}_{k+1}^{p-} = \sum_{i=0}^{2N} \left(w_m^{(i)} \mathbf{X}_{i,k+1}^{p-} \right)$$

$$\mathbf{P}_{pp}^- = \sum_{i=0}^{2N} w_m^{(i)} \left(\mathbf{X}_{i,k+1}^{p-} - \hat{\mathbf{x}}_{k+1}^{p-} \right) \left(\mathbf{X}_{i,k+1}^{p-} - \hat{\mathbf{x}}_{k+1}^{p-} \right)^T .$$

The weights are defined as

$$w_m^{(0)} = \frac{1}{100}, i = 0$$

$$w_m^{(i)} = \frac{1 - w_m^{(0)}}{2N_x}, i = 1, \dots, 2N$$

.

Remaining off-diagonal terms of the state covariance may be found from the propagated sigma points of two corresponding agents; that is

$$\mathbf{P}_{pq}^- = \sum_{i=0}^{2N} w_m^{(i)} \left(\mathbf{X}_{i,k+1}^{p-} - \hat{\mathbf{x}}_{k+1}^{p-} \right) \left(\mathbf{X}_{i,k+1}^{q-} - \hat{\mathbf{x}}_{k+1}^{q-} \right)^T . \quad (22)$$

3.2 Measurement Update Equations

For the numerical simulations which follow, measurements are assumed to be cyclically intermittent, and non-exhaustive. For instance, for the five-agent example, intrateam slant-range measurements are chosen in the sequence

$$\begin{Bmatrix} p \\ q \end{Bmatrix} \in \begin{bmatrix} 2 & 3 & 4 & 5 & 5 \\ 1 & 2 & 3 & 4 & 1 \end{bmatrix}, \tag{23}$$

selecting from 5 of the 10 possible combinations. Ground references are chosen in the corresponding sequence

$$\{k\} \in [1 \quad 2 \quad 2 \quad 3 \quad 1] .$$

Heading angles are taken from agent q in Eq. 23 except for the last instance when ψ_5 is selected.

At each measurement cycle, a vector of three measurements is assembled consisting of one slant-range measurement between agents, one agent heading angle, and one ground-reference slant range. The measurement vector is

$$\mathbf{y} = \begin{Bmatrix} \sqrt{(x_p - x_q)^2 + (y_p - y_q)^2} \\ \psi_q \\ \sqrt{(x_k - x_q)^2 + (y_k - y_q)^2} \end{Bmatrix} = \begin{Bmatrix} \rho_{pq} \\ \psi_q \\ \rho_{kq} \end{Bmatrix} \tag{24}$$

for planar motion or

$$\mathbf{y} = \begin{Bmatrix} \sqrt{(x_p - x_q)^2 + (y_p - y_q)^2 + (z_p - z_q)^2} \\ \psi_q \\ \theta_q \\ V_q \\ \sqrt{(x_k - x_q)^2 + (y_k - y_q)^2 + (z_k - z_q)^2} \\ z_q \end{Bmatrix} = \begin{Bmatrix} \rho_{pq} \\ \psi_q \\ \theta_q \\ V_q \\ \rho_{kq} \\ z_q \end{Bmatrix} \tag{25}$$

for spatial motion. In order to find a distribution of measurements corresponding to the sigma points $\mathbf{X}_{k+1}^{p-}$, $\mathbf{X}_{k+1}^{q-}$, the measurement vector is evaluated once for each column of the sigma points.

$$\mathbf{Y}_{i,k+1}^{-} = \mathbf{h}\left(\mathbf{X}_{i,k+1}^{p-}, \mathbf{X}_{i,k+1}^{q-}\right) . \tag{26}$$

Since range-only measurements involve the states of just two agents at a time, only the sigma points corresponding to agents p and q are required for this step. The measurement noise model can then be added as a batch $\mathbf{Y}_{k+1}^{-} = \mathbf{Y}_{k+1}^{-} \pm \sqrt{\mathbf{R}}$.

The a priori measurement prediction, covariance, and cross covariance can then be found by the weighted sums

$$\hat{\mathbf{y}}_{k+1}^{-} = \sum_{i=0}^{2N} \left(w_m^{(i)} \mathbf{Y}_{i,k+1}^{-} \right) \tag{27}$$

$$\mathbf{S} = \sum_{i=0}^{2N} w_m^{(i)} \left(\mathbf{Y}_{i,k+1}^{-} - \hat{\mathbf{y}}_{k+1}^{-} \right) \left(\mathbf{Y}_{i,k+1}^{-} - \hat{\mathbf{y}}_{k+1}^{-} \right)^T \tag{28}$$

$$\mathbf{P}_{py}^{-} = \sum_{i=0}^{2N} w_m^{(i)} \left(\mathbf{X}_{i,k+1}^{p-} - \hat{\mathbf{x}}_{k+1}^{p-} \right) \left(\mathbf{Y}_{i,k+1}^{-} - \hat{\mathbf{y}}_{k+1}^{-} \right)^T . \tag{29}$$

The Kalman gain for agent p is given by

$$\mathbf{K}^p = \mathbf{P}_{py}^{-} \mathbf{S}^{-1} . \tag{30}$$

In order to distribute the calculations across the formation, the following scheme is followed. Among the pair collecting the intra-agent slant range, one is designated lead p and the other is wing q. Quantities $\mathbf{Y}_{i,k+1}^{-}$, $\hat{\mathbf{y}}_{k+1}^{-}$, $\mathbf{S}$, $\mathbf{P}_{py}^{-}$, and $\mathbf{K}^p$ are computed as shown in Eqs. 26, 27, 28, 29, and 30, and $\mathbf{Y}_{i,k+1}^{-}$, $\hat{\mathbf{y}}_{k+1}^{-}$, and $\mathbf{S}$ are shared with the formation. If there are n agents, then after lead computes and transmits, the n-1 wingmen must compute $\mathbf{K}^q$, $\mathbf{P}_{qy}^{-}$, and $\mathbf{P}_{qr}^{-}$ using Eqs. 22, 29, and 30 with the appropriate modifications. Off-diagonal blocks of $\mathbf{P}^{+}$ are then computed from subsets of Eq. 8, and reflected across the diagonal.

$$\mathbf{P}_{pq,k+1}^{+} = \mathbf{P}_{pq,k+1}^{-} - \mathbf{K}^p \mathbf{S} \mathbf{K}^{qT} \tag{31}$$

$$\hat{\mathbf{x}}_{k+1}^{p+} = \hat{\mathbf{x}}_{k+1}^{p-} + \mathbf{K}^p (\mathbf{y}_{k+1} - \hat{\mathbf{y}}_{k+1}) . \tag{32}$$

3.2.1 Data Flow for Distributed Computation, Minimal Measurements

Figure 2 illustrates the communication required among five agents navigating cooperatively in 3-D with a minimal set of measurements for observability. If the team uses a minimal measurement vector, then $\mathbf{y} = [\rho_{pq} \quad \rho_{kp} \quad z_p]^T$, where p and q are cyclically assigned the values from the following set

$$\boldsymbol{\vartheta} = \begin{bmatrix} 1 & 2 & 3 & 4 & 5 \\ 2 & 3 & 4 & 5 & 1 \end{bmatrix} \tag{33}$$

$$\begin{Bmatrix} p \\ q \end{Bmatrix} = \boldsymbol{\vartheta}_i, \; i = \mathrm{mod}(k, 5) + 1 \, . \tag{34}$$

Altitude may be measured locally with an expected variance of approximately 1 m.[12] Estimation of agent position in 3-D space is much better with an onboard barometric altimeter as opposed to an onboard airspeed indicator.

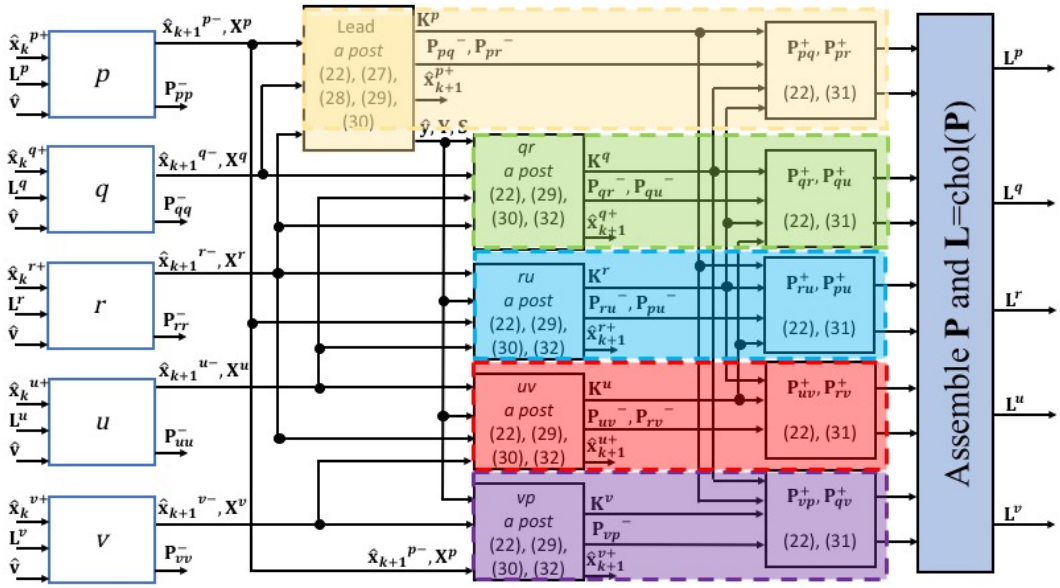

Fig. 2 Data flow for the distributed UKF algorithm with five agents. Boxes on far left represent each agent's prior predictions. Colored highlighted boxes define the total posterior computational load for each agent. The agent *p* is designated lead, and takes slant-range measurements from *q* and possibly *r* to assemble the measurement vector. Predicted state distributions are transmitted via the buses on the left for measurement vector predictions and a priori cross covariances. Kalman gain blocks are transmitted over the bus on the right to enable each agent to compute two off-diagonal blocks of the a posteriori system covariance matrix.

Figure 2 shows the data flow for filter updates. First, given the rows of **L** and $\hat{\mathbf{x}}$ corresponding to each agent, the plant dynamics are used to predict the a priori state distribution and diagonal blocks of the covariance. Next, agent *p* is designated the lead and as such assembles the measurement vector and makes measurement predictions based upon the predicted state distributions from agents *p* and *q*. It is then able to compute the measurement prediction mean, $\hat{\mathbf{y}}$, covariance, **S,** Kalman gain, $\mathbf{K}^p$, and cross covariance $\mathbf{P}_{pq}^-$, plus posterior state estimate and covariance $\hat{\mathbf{x}}^{p+}$, $\mathbf{P}_{pp}^+$. Measurement mean, distribution, and covariance are passed on to all agents allowing each agent in turn to compute its Kalman gain and prior cross covariance.

Once all Kalman gains are determined, each agent must receive two additional Kalman gains and one additional state mean and distribution to propagate two posterior off-diagonal blocks. Note that agent roles are redefined at each time step according to Eq. 34. Thus, agent 2 becomes lead at time k=1 and so on. In the five-agent case, there are 5 diagonal and 10 off-diagonal blocks, so dividing the workload equally requires each agent to compute one diagonal and two off-diagonal blocks. For larger formations, the number of off-diagonal blocks exceeds $2n$, so the distributed workload must increase accordingly.

3.2.2 Data Flow for Distributed Computation, Redundant Measurements

To enhance navigational performance, suppose a second intrateam measurement is included with each update; that is $\mathbf{y} = [\rho_{pq} \quad \rho_{pr} \quad \rho_{kp} \quad z_p]^T$, where every five time steps, the roles are assigned cyclically from the set

$$\begin{Bmatrix} p \\ q \\ r \end{Bmatrix} \in \begin{bmatrix} 1 & 2 & 3 & 4 & 5 \\ 2 & 3 & 4 & 5 & 1 \\ 3 & 4 & 5 & 1 & 2 \end{bmatrix}. \tag{35}$$

Figure 2 illustrates the data flow for UKF cooperative navigation under this scheme. As before, each agent propagates the distribution given by corresponding rows of $\mathbf{L}$ and $\hat{\mathbf{x}}$ through its dynamics to determine the prior state prediction, covariance, and distribution. Lead agent p then assembles the measurement vector and makes measurement predictions based upon the state distributions of agents p, q, and r. It is then able to also compute the off-diagonal priors $\mathbf{P}_{pq}^{-}$ and $\mathbf{P}_{pr}^{-}$, the Kalman gain, $\mathbf{K}^p$, diagonal posterior $\mathbf{P}_{pp}^{+}$, measurement mean and covariance, $\hat{\mathbf{y}}$ and $\mathbf{S}$, respectively. The measurement distribution, mean, and covariance are then passed to the wingmen who in turn compute their Kalman gains, covariance posterior, and two cross-covariance priors. Once the Kalman gains are computed, each agent must receive two additional Kalman gains. Each wingman must also receive one additional agent state distribution in order to compute its assigned second cross covariance. Finally, the entire system covariance matrix must be assembled for Cholesky factorization as described in Dinh and Kia.[8]

4. Results

Results from planar and spatial simulations are shown here. Sections 4.1 and 4.2 describe the outcome of applying the algorithm to a contrived scenario consisting of robots navigating in a plane. Sections 4.3, 4.4, and 4.5 describe the performance of the algorithm when applied to projectiles in 3-D flight at realistic speeds. Spatial results are based upon a high-fidelity 6-degree-of-freedom simulation of

10 Army-Navy finner (ANFIN) projectiles cooperatively attacking a target area used previously.[9,13]

4.1 Three Agents, Distributed EKF and UKF

A three-agent three-landmark scenario was simulated to compare performance of the distributed EKF and UKF with range-only measurements. One of three agents is polled each time step in sequence 2, 3, 1, 2, 3, …. Thus, for a simulation sampling rate of 100 Hz, measurements are sampled an effective rate of 33 Hz. Each agent measures one Euclidean distance to a teammate, one Euclidean distance to a landmark, and its local heading angle. All measurements are corrupted with Gaussian noise with $E[\mathbf{w}] = 0$ and $\sigma[\mathbf{w}] = 0.1$.

In Figure 3, performance of the distributed EKF and UKF is compared for the three-agent planar scenario. Figure 3a shows a bird's-eye view of the three agents' actual and estimated trajectories in the plane. Figure 3b shows the actual and estimated x coordinates, and Fig. 3c shows the actual and estimated y coordinates. Figure 3d shows the actual and estimated heading angles.

The effect of large additive noise is evident in Fig. 3d; however, the filters have reduced its effect considerably from $\sigma[\mathbf{w}] = 0.1$, to $\sigma[\boldsymbol{\psi}] = [0.016 \quad 0.032 \quad 0.021]$ for the EKF and $\sigma[\boldsymbol{\psi}] = [0.031 \quad 0.036 \quad 0.030]$ for the UKF. Similar but reduced noise is apparent in the estimated Cartesian coordinates. Performance of the two filters is comparable with the EKF showing more accurate estimates for the Cartesian coordinates, and the UKF showing faster convergence for the heading angle estimate.

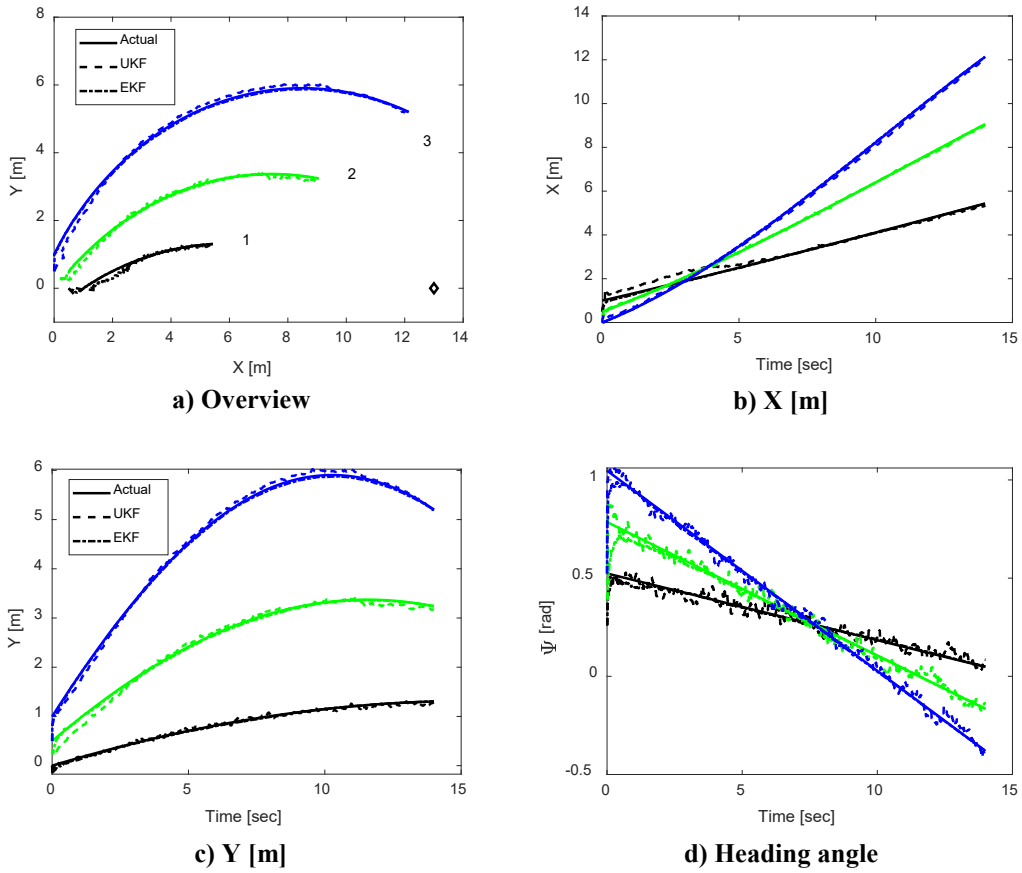

Fig. 3 Performance comparison of distributed EKF and distributed UKF, three-agent scenario, large sensor noise

4.2 Four Agents, Planar Motion

The planar experiment was repeated, appending a fourth agent but sharing the three landmarks. Again, agents took turns contributing their observations, and covariance updates were distributed across the formation as previously discussed. Thus, each agent took the lead role only once every four time steps. With four agents, a total of six off-diagonal blocks must be propagated, so two agents had to assume the additional computational burden. The default workload is to propagate a diagonal block and either a superdiagonal block or corner block as shown in Fig. 1.

Figure 4 shows the performance of the UKF and EKF for the four-agent scenario. Again, with large additive noise, performance is similar to the three-agent scenario, although the effective measurement sampling rate is now only 25 Hz.

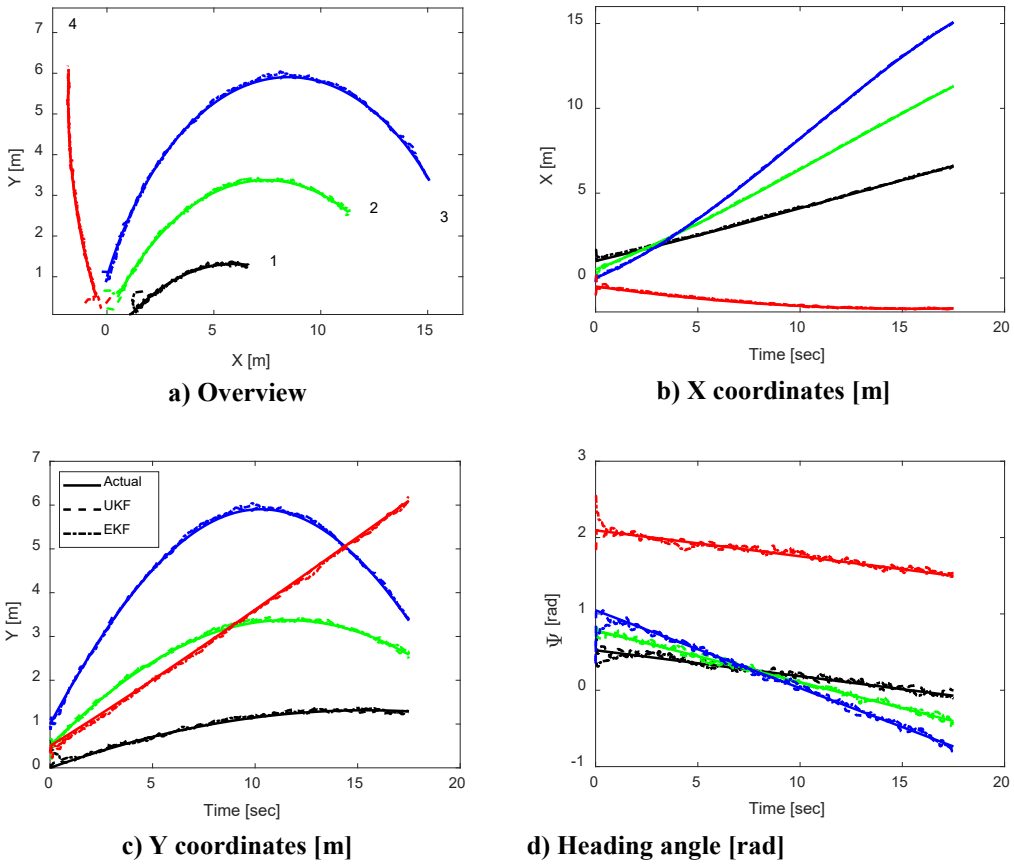

Fig. 4 Performance comparison distributed UKF against distributed EKF, four agents

4.3 Spatial Motion, EKF Compared with UKF

Due to the linearization of the EKF, six measurements per agent were required for spatial estimation as shown in Section 3.2. The UKF can satisfy observability with fewer measurements as will be shown in Section 4.4. A minimum formation size of four agents was used to confirm observability of each distributed scheme with intermittent measurements. The truth model was taken from a high-fidelity simulation of 10 ANFIN projectiles cooperatively attacking a target area.[13] Figure 5 shows the scenario from separation point, near apogee, to target impact. An inlay zoom plot depicts the target area, and desired "bowling pin" pattern. Eight of the 10 trajectories are depicted, and smaller formations will be selected from these eight for the spatial results of this work.

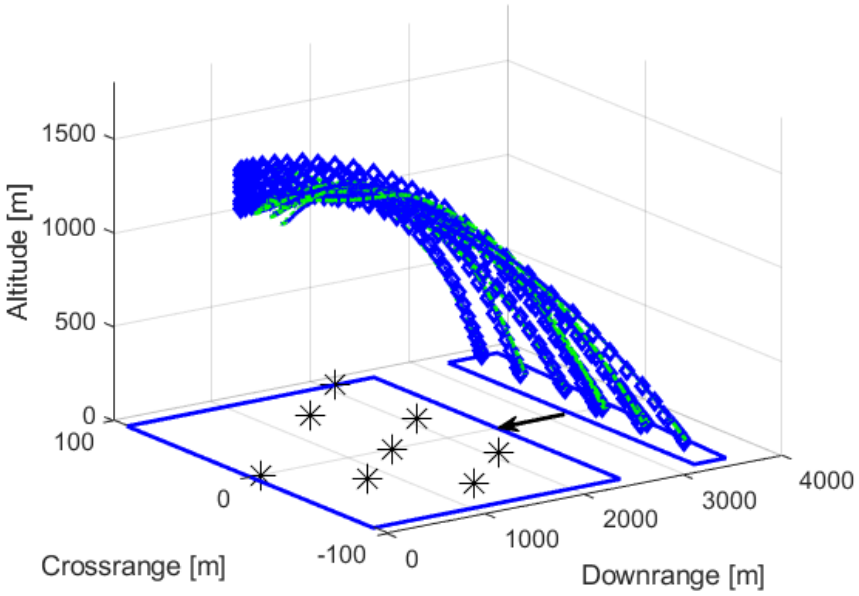

Fig. 5 Spatial scenario, from Burchett[10]

Figure 6 displays the estimation error for the EKF and UKF when using six measurements per observation for a team of six agents. EKF estimation error is plotted using a dash–dot line, and UKF estimation error is shown as a solid line. Performance is comparable for the two methods, with the UKF showing smaller initial transients in estimation error.

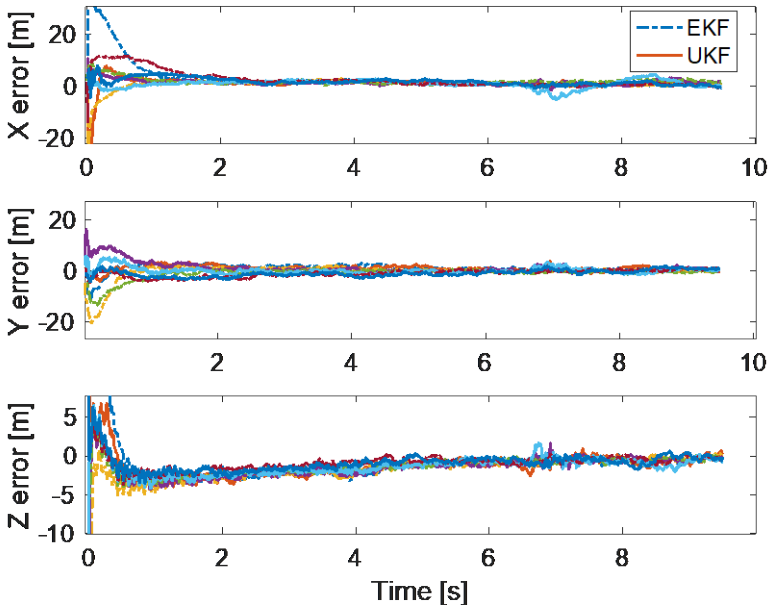

Fig. 6 Performance of the distributed EKF and UKF, four agents in spatial flight, six measurements per agent

4.4 Spatial Motion, Minimal Measurements

In order to reduce onboard sensor requirements, dimensions of state and measurement distributions, and thus communication requirements, UKF simulations were repeated with the measurement vector defined in Section 3.2.1. Observability using such a measurement scheme was previously demonstrated for a centralized filter in Burchett.[9] Thus, this investigation seeks to confirm that observability is not adversely affected by distributing the algorithm, or limiting measurements to intermittent but consistent availability.

A formation in 3-D flight must have at least four agents and measure at least four ground stations to achieve observability with the three-measurements-per-agent and six-states-per-agent model.

Figures 7 and 8 show the time history of estimation errors for a team of four agents navigating with just three measurements per agent. Figure 6 shows the spatial coordinates. The estimation errors are shown as colored lines. Zero-mean three-sigma boundaries are shown on the x and y plots as dashed black lines. Lines for all four agents are depicted based upon the corresponding diagonal element of the state covariance matrix. Three-sigma boundaries are not shown for altitude to reduce clutter.

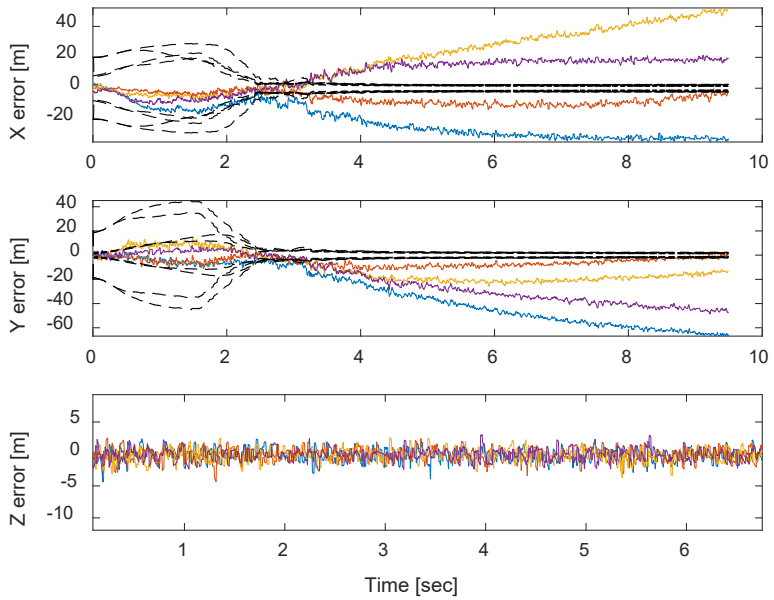

Fig. 7 Performance of the distributed UKF, four agents in spatial flight, three measurements per agent

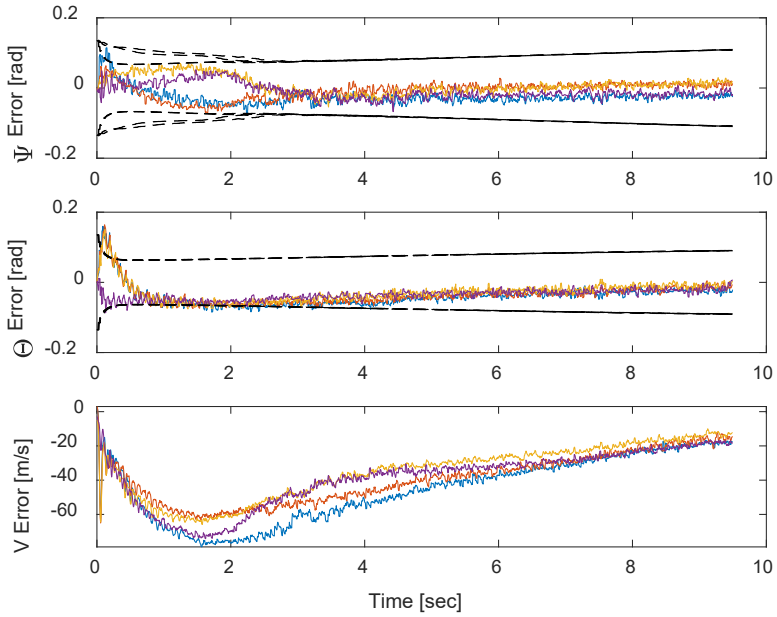

Fig. 8 Performance of the distributed UKF, four agents in spatial flight, three measurements per agent. Convergence of unmeasured state estimates heading angle (ψ), flight path angle (θ), and total velocity (V).

The x and y estimate errors remain inside the three-sigma boundaries for about 2.5 s of flight—after this, the covariance estimate is overly optimistic resulting in diverging errors and inconsistent estimates. Altitude errors are small for all agents due to direct altitude measurements.

Figure 8 shows the heading angle, flight path angle, and forward speed estimate errors. Three-sigma bounds are shown for ψ and θ. ψ and θ estimates are consistent with θ errors showing some negative bias for the first 4 s. Forward speed estimates lag the truth values due to the absence of a direct measurement.

Overall performance with minimal measurements in spatial flight is unsatisfactory which will be revisited in the next section.

4.5 Spatial Motion, Redundant Measurements

Since estimation performance was unsatisfactory with minimal measurements, the UKF spatial simulations were repeated using an additional slant-range measurement with each observation as shown in Section 3.2.2. Simulations for four, five, and six agents navigating in 3-D were repeated 20 times each to quantify performance apart from random effects between individual trials. Terminal estimation errors for these tests are recorded in Fig. 9 and in the Appendix, Table A-1. To reduce performance to one metric per direction per strategy, terminal errors were averaged across the formation using root mean square for each trial. The box

plots in Fig. 8 display the distribution of terminal errors for the four-, five-, and six-agent cases using minimal (min) and redundant (red) measurement schemes. The top subplot shows the distributions for the minimal measurement trials. Its axis is scaled to contain all features of the box plots, causing the 25th, 50th, and 75th percentiles to be nearly coincident for several quantities shown. The four- and six-agent cases have downrange and cross-range errors exceeding 10 m for all cases. All cases have altitude errors below 2 m due to direct altitude measurement with an assumed instrument accuracy of σ = 1 m. The five-agent case has median downrange and cross-range errors of about 4 m with the largest errors remaining below 8 m.

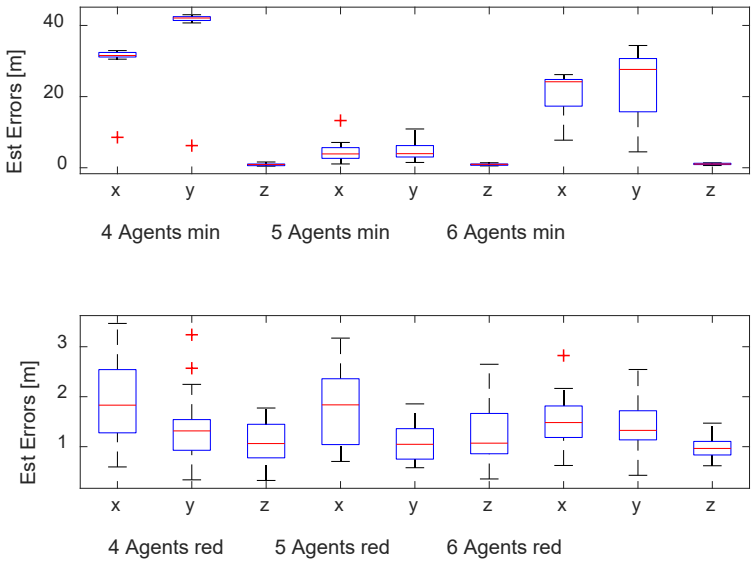

Fig. 9 Box plots comparing the performance of minimal (min) three measurements per agent

The bottom subplot shows the distributions for the redundant measurement trials. All features of all boxes lie between 0.5 and 3.0 m. Median errors for all cases except for the five-agent downrange are below 2 m.

Figures 10 and 11 show the time history of estimation errors for a team of four agents navigating with four measurements per agent. Three-sigma bounds are shown for x, y, ψ, θ, and V. All estimates converge to small errors after about 2 s, and all except V remain within the 3σ bounds.

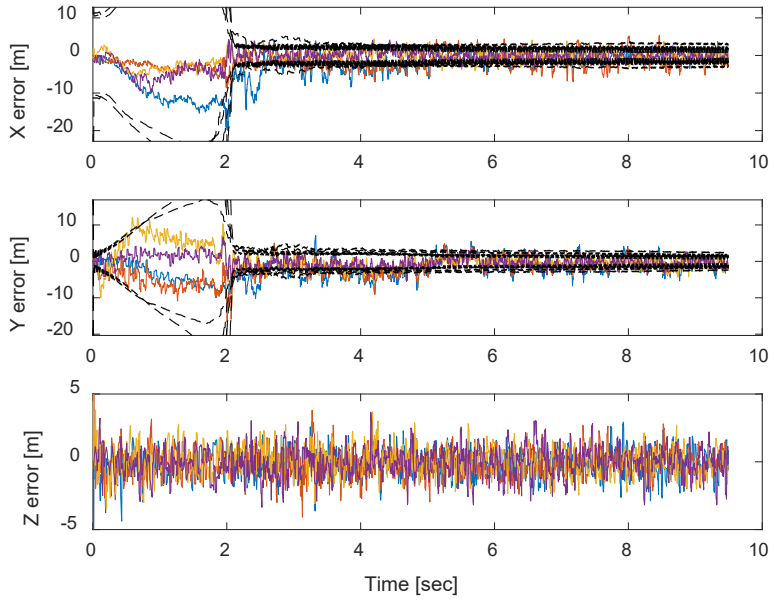

Fig. 10 Performance of the distributed UKF, four agents in spatial flight, four measurements per agent

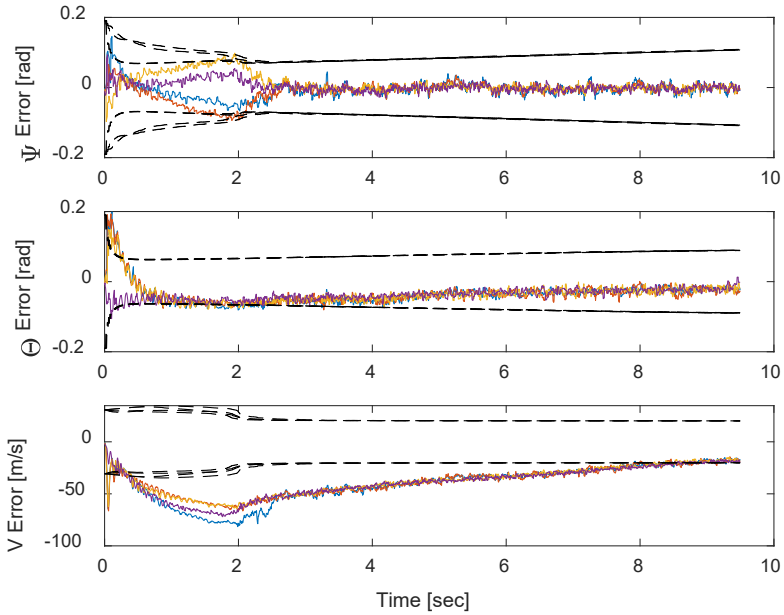

Fig. 11 Performance of the distributed UKF, four agents in spatial flight, four measurements per agent. Convergence of unmeasured state estimates heading angle (ψ), flight path angle (θ) and total velocity (V).

Figures 12 and 13 depict the estimation error time history for a team of six agents using four measurements per agent. Performance is very similar to the four-agent case except that spatial coordinates converge somewhat faster.

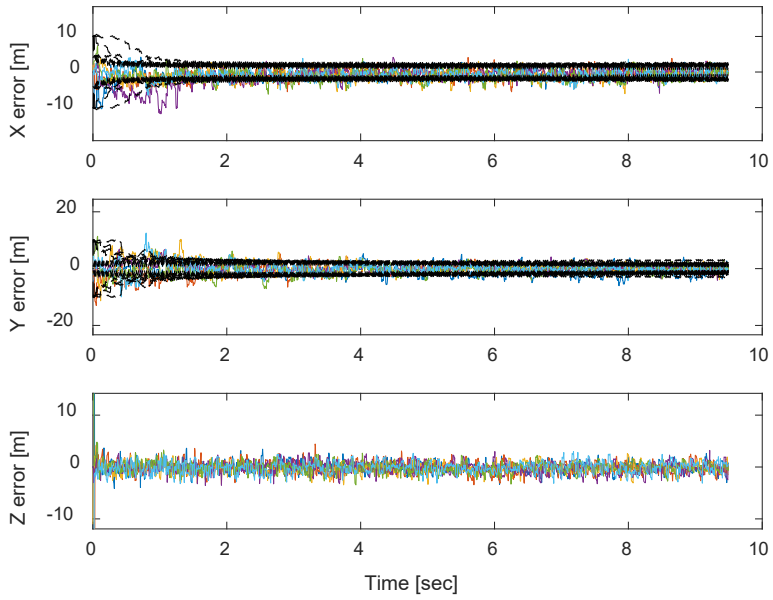

Fig. 12 Typical performance of the distributed UKF, six agents in spatial flight, four measurements per agent

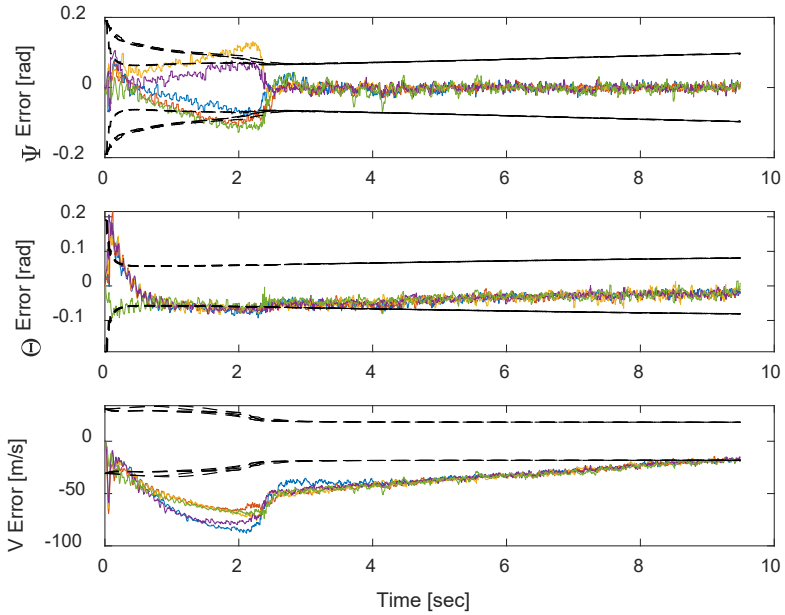

Fig. 13 Typical performance of the distributed UKF, six agents in spatial flight, four measurements per agent. Convergence of unmeasured state estimates heading angle (ψ), flight path angle (θ) and total velocity (V).

5. Conclusion

This report has reviewed the formulation of the distributed EKF for cooperative localization with range-only measurements. A distributed set of unscented filters was also developed. The algorithms have been presented in a format that is readily expanded to teams of arbitrary size, and results were shown for teams as large as six. Data flow among agents for the distributed UKF was specified for teams of up to five agents.

In planar motion, both types of filters performed well with a common measurement scheme. In spatial motion, the EKF required six measurements per agent to achieve observability for a six-state-per-agent system model. The UKF demonstrated observability with as few as three measurements per agent, but required four measurements per agent for satisfactory performance. Agents are able to cooperatively determine their position with slant-range measurements to one ground station and two neighboring agents plus onboard barometric sensing of altitude. Local sensing of altitude was found to be essential to a consistent estimation scheme.

6. References

1. He L, Bai P, Liang X, Zhang J, Wang W. Feedback formation control of UAV swarm with multiple implicit leaders. Aerosp Sci Technol. 2018;72:327–334. doi: 10.1016/j.ast.2017.11.020.

2. Vu R, Rahmani A. Analysis of a distributed estimation and control scheme for formation flying spacecraft. Aerosp Sci Technol. 2018;73:232–238. doi: 10.1016/j.ast.2017.10.028.

3. Wang W, Bai P, Liang X, Zhang J, He L. Performance analysis and path planning for UAVs swarms based on RSS measurements. Aerosp Sci Technol. 2018;81:157–166. doi: 10.1016/j.ast.2018.07.021.

4. Xu M, Liang Y, Fu X. Formation flying on quasi-halo orbits in restricted sun–earth/moon system. Aerosp Sci Technol. 2017;67:118–125.

5. Roumeliotis SI, Bekey GA. Distributed multirobot localization. IEEE Trans Robo Autom. 2002;18(5):781–795.

6. Julier SJ, Uhlmann JK. Unscented filtering and nonlinear estimation. Proceedings of the IEEE. March 2004;92(3):401–422.

7. Lee DJ. Unscented information filtering for distributed estimation and multiple sensor fusion. AIAA Guidance, Navigation and Control Conference and Exhibit; 2008 Aug 18–21; Honolulu, HI. AIAA Paper 2008-7426.

8. Dinh V, Kia SS. A server-client based distributed processing for an unscented Kalman filter for cooperative localization. 2015 IEEE International Conference on Multisensor Fusion and Integration for Intelligent Systems (MFI); 2015 Sep 14–16; San Diego, CA. p. 43–48. doi: 10.1109/MFI.2015.7295743.

9. Burchett BT. Unscented kalman filters for range-only cooperative localization of swarms of munitions in three-dimensional flight. Aerosp Sci Technol. 2019;85:259–269. doi: 10.1016/j.ast.2018.12.015.

10. Burchett BT. A centralized extended Kalman filter for cooperative localization of munition swarms. Proceedings of the AIAA Aviation Forum 2019; Dallas, TX; 2019 June 17–21.

11. Maier RS, Rohaly TF, Fickie KD, Advani SG. A fast numerical method for isothermal resin transfer mold filling. Aberdeen Proving Ground (MD): Army Research Laboratory (US); 1994 Nov. Report No.: ARL-TR-610.

12. Sabatini AM, Genovese V. A stochastic approach to noise modeling for barometric altimeters. Sensors (Basel). 13(11):15692–15707. doi: 10.3390/S131115692.

13. Burchett BT. Cooperative navigation for large swarms of munitions in three-dimensional flight. AIAA Modeling and Simulation Technologies Conference, AIAA SciTech Forum; 2018 Jan 8–12; Kissimmee, FL. AIAA Paper 2018-0433.

Appendix. Additional Statistics for Spatial Simulations

The simulations for four, five, and six agents navigating in 3-D were repeated 20 times each to quantify performance apart from random effects between individual trials. Terminal estimation errors for these tests are recorded in Table A-1. To reduce performance to one metric per direction per strategy, terminal errors were averaged across the formation using root mean square (RMS) for each trial, then mean and standard deviation were computed across 20 trials. The values in Table A-1 indicate that the algorithm performance was best for six agents with redundant measurements and worst for four agents with minimal measurements.

Table A-1 Performance of the distributed unscented Kalman filter (UKF) for spatial flight, using three measurements per agent (min) or four measurements per agent (red)

No. agents	Terminal estimation errors [m], RMS across formation, then mean, std. deviation for N=20 trials each					
	$\boldsymbol{E}[\tilde{\boldsymbol{x}}_\infty]$	$\boldsymbol{E}[\tilde{\boldsymbol{y}}_\infty]$	$\boldsymbol{E}[\tilde{\boldsymbol{z}}_\infty]$	$\boldsymbol{\sigma}[\tilde{\boldsymbol{x}}_\infty]$	$\boldsymbol{\sigma}[\tilde{\boldsymbol{y}}_\infty]$	$\boldsymbol{\sigma}[\tilde{\boldsymbol{z}}_\infty]$
4 ship min	30.63	40.20	0.89	5.24	8.02	0.34
4 ship red	1.91	1.37	1.05	0.79	0.69	0.40
5 ship min	4.40	4.81	0.90	2.76	2.60	0.23
5 ship red	1.77	1.09	1.28	0.72	0.36	0.62
6 ship min	20.75	23.68	1.06	6.50	9.48	0.22
6 ship red	1.47	1.42	0.98	0.55	0.52	0.22

List of Symbols, Abbreviations, and Acronyms

3-D	three-dimensional
ANFIN	Army–Navy finner
GPS	global positioning system
sIF	sigma point Information Filter
UAV	unmanned aerial vehicle
UKF	unscented Kalman filter

Nomenclature

$\{x, y, \psi\}$	agent pose in planar motion in ground fixed frame [m, m, rad]
$\{z, V, \gamma\}$	additional pose states for spatial motion [m, m/s, rad]
$\{p,q,r\}$	agent numbers in the first team of three
$\{u,v,w\}$	agent numbers in the second team of three
k	simulation sample number / ground reference number
$\mathbf{x}$	system state vector
$\mathbf{y}$	system measurement vector
$\mathbf{f}(.)$	nonlinear system state dynamics model
$\mathbf{h}(.)$	nonlinear system measurement model
$\mathbf{A}$	system dynamics Jacobian matrix
$\mathbf{H}$	system measurement Jacobian matrix
$\mathbf{K}$	Kalman gain
$\mathbf{P}$	system state estimation covariance
$\mathbf{Q}$	process noise covariance matrix
$\mathbf{R}$	measurement noise covariance matrix
$\mathbf{S}$	system measurement covariance
$\mathbf{v}$	additive process noise vector

w	additive measurement noise vector
Φ	state transition matrix

Subscript

p	rows corresponding to agent *p*
pq	block with rows corresponding to agent *p*, columns to agent *q*
k	time sample number

Superscript

-	a priori
+	a posteriori
p	block with rows corresponding to agent *p*
T	matrix transpose
i	matrix row space, column of sigma point distribution
j	matrix column space

1 (PDF)	DEFENSE TECHNICAL INFORMATION CTR DTIC OCA
1 (PDF)	CCDC ARL FCDD RLD CL TECH LIB
1 (PDF)	GOVT PRINTG OFC A MALHOTRA
1 (PDF)	RHIT B BURCHETT
20 (PDF)	CCDC ARL FCDD RLW C C KRONINGER FCDD RLW LE P WEINACHT VA BHAGWANDIN I CELMINS J DESPIRITO LD FAIRFAX FE FRESCONI FCDD RLW LF M ILG B ALLIK TG BROWN E BUKOWSKI BS DAVIS M DON D EVERSON M HAMAOUI B KLINE J MALEY C MILLER B NELSON B TOPPER